The FASEB Journal express article10.1096/fj.04-2834fje. Published online December 13, 2004.

Enhanced macromolecular diffusion in brain extracellular space in mouse models of vasogenic edema measured by cortical surface photobleaching

Marios C. Papadopoulos,* Devin K. Binder,† and A. S. Verkman*

Departments of *Medicine and Physiology, and †Neurological Surgery, University of California at San Francisco, San Francisco CA 94143, U.S.A.

Corresponding author: Alan S. Verkman, 1246 Health Sciences East Tower, Cardiovascular Research Institute, University of California, San Francisco San Francisco, CA 94143-0521, U.S.A. E-mail: verkman@itsa.ucsf.edu; http://www.ucsf.edu/verklab

ABSTRACT

Diffusion of solutes and macromolecules in brain extracellular space (ECS) is important for normal brain function and efficient drug delivery, and is thought to be impaired in edematous brain. Here we measured the diffusion of an inert macromolecular fluorescent marker (FITC-dextran, 70 kDa) in the ECS by fluorescence recovery after photobleaching after staining the exposed cerebral cortex in vivo. In a brain tumor model of vasogenic (leaky capillary) edema, FITC-dextran diffusion was reduced more than fourfold in hypercellular tumor and surrounding astrogliotic tissue; however, diffusion in brain away from the tumor was ~30% faster than in normal contralateral brain. The increased diffusion was abolished by dexamethasone pretreatment. Enhanced ECS diffusion was also found in uninjured brain near a region of leaky brain vessels produced by focal cortical freeze injury. In contrast, ECS diffusion was slowed more than sixfold in cytotoxic brain edema caused by anoxia. Diffusion results were related semiquantitatively to ECS volume fraction and matrix viscosity from in vitro photobleaching studies in a model system consisting of silica particles in a fluorescent water/glycerol matrix. Our data provide in vivo evidence for enhanced ECS diffusion in vasogenic brain edema, yet greatly slowed diffusion in cytotoxic edema and in and around tumors.

Key words: brain swelling • blood-brain barrier • brain tumor • fluorescence • FRAP

The extracellular space (ECS) comprises ~20% of brain tissue volume and is important for many brain processes, including neuron-glia communication, diffusion of ions, neurotransmitters and metabolites, as well as drug delivery. Brain edema, defined as a net increase in brain tissue water content, is expected to alter ECS size, thus profoundly influencing normal brain function. It is currently unclear how different types of brain edema affect the diffusion of molecules in the ECS.

Brain edema occurs in diverse pathologies, including brain tumor, infection (brain abscess and meningitis), stroke, head injury, and toxic/metabolic states (e.g., liver failure, sepsis, lead intoxication) (1–6). Brain edema increases intracranial pressure (ICP), potentially leading to

brain ischemia, herniation, and death. Treatment options for brain edema have changed little over 80 years (7), being limited to craniectomy (to decompress brain parenchyma), intravenous hyperosmotic solutions (to reduce overall brain water content), and corticosteroids (for brain tumor edema) (3, 8, 9).

Historically, brain edema has been classified into "cytotoxic" and "vasogenic" types (6). Cytotoxic edema, as observed in the early phase of hypoxic/ischemic injury, is associated with cellular (primarily glial cell) swelling (2) and can be produced experimentally by acute water intoxication (10). Vasogenic edema, classically associated with brain tumors, is produced by water entry into brain tissue across leaky blood-brain and blood-tumor barriers (4). Using three experimental models of vasogenic edema, including intraparenchymal fluid infusion, cortical freeze injury, and tumor implantation, we found recently that mice lacking the water channel aquaporin-4 (AQP4) had elevated ICP and brain water, and worse clinical outcome (11). It was postulated that impaired water escape across the AQP4-rich brain-CSF barrier reduced the removal of excess fluid, causing water accumulation in the brain ECS.

The purpose of this study was to test the hypothesis that vasogenic brain edema causes ECS expansion, whereas cytotoxic edema produces ECS contraction as manifest by altered diffusion of an inert macromolecule. The standard method for measuring ECS parameters in rodent brain is the tetramethylammonium (TMA^+) method (12, 13), but this is largely restricted to brain slices. Vasogenic edema can only be studied in vivo because brain slices lack a circulation and their ECS is in continuity with the bathing solution. The TMA^+ method is not easily applied to measurements in vivo and has several other limitations, including direct micropipette invasion of the measurement site, sensitivity of the monitoring micropipette to both [TMA^+] and [K^+], and difficult-to-justify assumptions in computing ECS diffusion from the complex kinetics of [TMA^+] following pulsed injection.

To overcome limitations of the TMA^+ method particularly for in vivo studies, we recently developed a noninvasive technique to measure molecular diffusion in the ECS (14). Brain ECS is loaded with a fluorescent dye, such as FITC-dextran, and diffusion is measured by fluorescence recovery after photobleaching. Loading is accomplished by exposing the brain, with dura intact but the bony skull removed, to an artificial CSF (aCSF) solution containing the fluorescent dye. After dye washing, brain surface photobleaching measurements are carried out in vivo with the mouse immobilized on a stereotactic frame on the stage of an upright laser microscope. The photobleaching data are interpreted quantitatively to yield dye diffusion coefficients and derived tortuosities, providing a measure of ECS expansion/contraction. Cortical photobleaching is uniquely useful for studies of vasogenic edema mechanisms because it is minimally invasive and suitable for measurements in in vivo models of vasogenic edema. We report here evidence for significant ECS expansion in brain tumor and cortical freeze-injury models of vasogenic brain edema, and ECS contraction in anoxic and toxic models of cytotoxic brain edema. The diffusion data are interpreted in terms of altered ECS properties by photobleaching measurements on a simple in vitro system in which cells/ECS are modeled by concentrated suspensions of micron-size silica particles in a fluorescent water/glycerol matrix.

MATERIALS AND METHODS

Mice

Experiments were performed on weight-matched (generally 25–30 g) male C57/BL6 mice. Protocols were approved by the University of California San Francisco Committee on Animal Research. Mice were anesthetized with 2,2,2-tribromoethanol (avertin, Sigma-Aldrich, St. Louis, MO) (i.p. 125 mg/kg) and immobilized in a stereotactic frame (Benchmark, Neurolab, St. Louis, MO). Additional avertin was given as needed to maintain an even depth of anesthesia. For tumor implantation and cold injury, the mouth bar was set at 5 mm and ear bars at 10 mm. Burr holes (1 mm diameter) were made with a high-speed micromotor drill (Model 3545, Foredom, Bethel, CT). Core temperature was maintained between 37 and 38°C using a heating lamp.

Dye loading for photobleaching measurements

After exposing the skull by midline skin incision, an atraumatic craniectomy was done using the micromotor drill to expose the intact cortical dura and underlying brain surface. The craniectomy margins were the coronal suture anteriorly, the lambdoid suture posteriorly, and the attachment of each temporalis muscle laterally. Following craniectomy, the skin flaps were held open with a cylindrical dam to create a pocket for dye loading (Fig. 1*A*).

The ECS was dye-loaded by 2–3 h incubation with aCSF (in mM: NaCl, 145; KCl, 4; $MgCl_2$, 1; $CaCl_2$, 2.5; KH_2PO_4, 1; glucose, 10; pH 7.4) containing FITC-dextran (70 kDa, 35 mg/ml). After loading, the dural surface was washed with dye-free aCSF, the skin flaps were removed, and the stereotactic frame was transferred to the stage of an upright epifluorescence microscope. Mice with cortical damage or inadequate fluorescence labeling (<10% of mice) were excluded from photobleaching measurements.

Fluorescence recovery after photobleaching

Photobleaching measurements were done on an apparatus described previously (15) after modification for confocal detection (14). Briefly, the first order beam of an argon ion laser (2 W at 488 nm) diffracted by an acousto-optic modulator was focused onto the surface of the mouse brain through a dichroic mirror (510 nm) and objective lens (Nikon ×50 air, numerical aperture 0.55, working distance 8 mm). Emitted fluorescence was filtered (510 nm long-pass) and detected by a photomultiplier. Confocal detection was achieved by positioning a 400 μm diameter precision pinhole (using an *xy* micropositioner) at the back focal plane. Fluorescence was sampled continuously over 200 ms before the bleach pulse, at rates of up to 1 kHz for 500 ms after bleaching, and then at 1 Hz (shutter opened for 20 ms per acquisition) for longer times (10–180 s). Fluorescence recovery curves, F(t), were analyzed by nonlinear least-squares regression using the semiempirical equation:

$$F(t) = (F_0 + [R(F–F_0) + F_0](t/ t_{1/2}))[1 + (t/t_{1/2})]^{-1}$$

where F is prebleach fluorescence, F_0 is fluorescence immediately after bleaching, R is the mobile fraction, and $t_{1/2}$ is the recovery half-time (16).

For in vivo measurements, the laser spot was focused onto the cortical surface. An adjustable mechanical arm fixed to the stereotactic frame was used to position a small (3-mm-diameter, 150-μm-thick) glass window on the cortical surface to dampen cardiorespiratory oscillations (Fig. 1*B*). Previous control studies indicated that the glass window did not affect diffusion measurements (14). Bleaching was accomplished by increasing laser illumination intensity ~4000-fold and bleach duration was set empirically (generally 1–5 ms) to achieve 40–50% reduction in fluorescence within the illuminated circular spot. F(t) from 3-8 different cortical spots were generally averaged per condition for each mouse. For in vitro measurements, solutions containing aCSF, FITC-dextran (70 kDa, 35 mg/ml), various concentrations of silica microbeads (median diameter 0.1 μm, Raede Advanced Materials, Reno, NV) and glycerol, were sandwiched between glass coverslips.

GFAP immunohistochemistry

Mouse brains were fixed in 10% formalin (Accustain, Sigma-Aldrich) overnight, processed through graded concentrations of ethanol, immersed in Citrisolv (Fisher Scientific, Los Angeles, CA), and embedded in paraffin. Tissue sections (7-μm-thick) were deparafinized in Citrisolv and rehydrated with graded ethanols. After blocking with goat serum, samples were incubated with a rabbit anti-GFAP polyclonal antibody (1:1000, Chemicon, Temecula, CA) and washed in PBS. Bound antibody was detected using the Vectastain Elite ABC kit (Vector Laboratories, Burlingame, CA) according to the manufacturer's instructions.

Brain tumor model

B16F10 melanoma cells (derived from C57/BL6 mice) (no. CRL-6475, ATCC, Manassas, VA) were grown in MEM supplemented with 10% fetal bovine serum. A burr hole was drilled 2.5 mm to the right and 0 mm caudal to the bregma. A 26-gauge needle attached to a gas-tight 10 μl Hamilton syringe was inserted through the burr hole 3 mm deep. Melanoma cells (10^5) suspended in 5 μl MEM was infused into the brain parenchyma over 2–5 min. The needle was removed, and the skin was sutured. Photobleaching experiments were done 5 days after implantation. In some experiments, mice received dexamethasone (0.8 mg/kg, i.p.) twice daily on days 3–5 after tumor cell implantation.

Cortical freeze injury model

The mouse head was immobilized in a stereotactic device, and a midline incision was made in the scalp to expose the sutures. An agarose disc (4.5-mm-diameter, 1-mm-thick) was placed over the right parietal bone. The tip of a 4.5-mm-diameter copper rod attached to a cold copper reservoir containing acetone/dry ice was positioned over the agarose disc, and the skull was compressed by 0.5 mm for 30 s. Photobleaching measurements were done 6 h after the cold injury.

Cytotoxic brain edema models

Before hypoxia, fluorescence recovery curves were obtained from at least three different cortical regions. Two models of cerebral hypoxia were used: 1) topical (cortical) hypoxia was produced by exposing the cerebral cortex to 10 mM KCN (in aCSF) for 5 min, and cortical photobleaching

was performed after 15 min, and 2) global hypoxia was produced by avertin overdose (500 mg/kg, i.p. bolus) to cause apnea. Fluorescence was recorded 5 min after the onset of apnea, at which time arterial blood gases were pH 6.83 ± 0.01, pO_2 = 17 ± 5 kPa, and pCO_2 = 107 ± 8 kPa.

Statistics

Data are presented as mean ± SE. Student's *t* test was used to compare two groups of variables and ANOVA followed by Student-Neumann-Keuls test for comparison of multiple group pairs. Statistical significance was taken as $P < 0.05$.

RESULTS

Cortical surface photobleaching measurements

Laser photobleaching was done to measure FITC-dextran diffusion in brain cortex in vivo. As shown in Figure 1*A*, the ECS was stained with FITC-dextran by incubation after removal of the bony skull, but with dura intact. During optical measurements a coverslip was gently applied to the dura to dampen cardiorespiratory oscillations (Fig. 1*B*). Figure 1*C* shows the brightly fluorescent brain and tumor surfaces in a mouse at 5 days after melanoma tumor cell implantation. Fluorescence was excluded from cortical blood vessels. Figure 1*D* shows FITC-dextran fluorescence in superficial cortical layers in a brain slice (150-µm-thick) cut just after dye loading. To investigate the cellular features that may be responsible for the very different diffusion characteristics of tumor vs. brain ECS as shown below, we examined GFAP-immunostained brain sections. Compared with normal cerebral cortex (Fig. 1*E*), tumor and peritumoral tissue showed a higher density of cells and cellular processes (Fig. 1*F*). No necrosis or hemorrhage was seen inside the tumor in the studies here.

Models of vasogenic and cytotoxic brain edema

Using the melanoma model described above, fluorescence recovery after photobleaching was measured at different sites: within tumor tissue, in peritumoral brain just outside of the tumor, in ipsilateral brain away from the tumor margin, and in contralateral brain (Fig. 2*A*). Separate studies were done in normal brains from nine mice without tumors. The site of diffusion measurement had a remarkable effect on fluorescence recovery as shown by representative recovery curves in Figure 2*A*, and as quantified by recovery half-times ($t_{1/2}$) and corresponding FITC-dextran diffusion coefficients (Fig. 2*B*). Compared with normal brain ($t_{1/2}$=277±13 ms), diffusion was significantly slowed inside the tumor ($t_{1/2}$=1.3±0.3 s) and in the peritumoral region ($t_{1/2}$=1.1±0.2 s). After photobleaching, the recovery of fluorescence at long times was complete in normal brain (98±2%), but significantly incomplete inside (78±5%) and around (79±4%) the tumor. Interestingly, FITC-dextran diffusion in the hemisphere ipsilateral to the tumor (but >2 mm away from the tumor margin) was significantly faster ($t_{1/2}$=210±21 ms), whereas diffusion in the contralateral hemisphere ($t_{1/2}$=294±7 ms) was not different from that in normal brain.

To test the hypothesis that FITC-dextran diffusion is accelerated in ipsilateral brain tissue because of ECS water accumulation by a vasogenic mechanism, we treated mice with brain tumors with dexamethasone, which is known to reduce brain tumor edema (17) and inhibit vessel leak (18, 19). After dexamethasone, FITC-dextran diffusion in ECS of ipsilateral cortex

($t_{1/2}$=294±10 ms) was reduced to that seen in normal brain; dexamethasone had no effect on FITC-dextran diffusion in the ECS of the contralateral hemisphere ($t_{1/2}$=293±18 ms) (Fig. 3).

Another well-established model of vasogenic edema, cortical freeze injury, was used to verify the generality of the apparent ECS expansion near a site of vascular leak. Transient contact of the cortical surface with a cold metallic probe caused opening of the blood-brain barrier, as evidenced by Evans blue extravasation within the region of contact and transient freeze (Fig. 4*A*, inset). Photobleaching measurements showed that FITC-dextran diffusion in the ECS of the hemisphere ipsilateral to the lesion (but >1 mm away from the lesion) was significantly enhanced ($t_{1/2}$=186±15 ms) compared with normal brain. Diffusion in the contralateral (uninjured) hemisphere ($t_{1/2}$=296±22 ms) did not differ significantly from that of normal brain (Fig. 4). There was complete recovery of fluorescence to the prebleach level in both hemispheres.

We also investigated the effect of cytotoxic edema on FITC-dextran diffusion in the ECS (Fig. 5), testing the hypothesis that acute cell swelling would reduce ECS volume and consequently slow FITC-dextran diffusion. In two models of cerebral hypoxia, a focal model produced by topical cyanide and a global model caused by apnea, FITC-dextran diffusion in the ECS was remarkably slowed by 6.7- and 8.2-fold, respectively. Hypoxia resulted in significantly incomplete recovery of fluorescence after photobleaching (76±8% for cyanide, 60±5% for apnea), suggesting the presence of "dead space microdomains" in which free FITC-dextran diffusion cannot occur.

In vitro model of brain ECS

As illustrated in Figure 6*A*, we hypothesize that in cytotoxic brain edema cell swelling produces a reduction in ECS size and the creation of dead space microdomains, resulting in restricted macromolecule diffusion in the ECS. In contrast, we postulate that vasogenic brain edema produces ECS expansion, resulting in enhanced macromolecular diffusion. To explore these ideas, we modeled the complex architecture of the ECS using suspensions of silica microbeads in fluorescently-stained water/glycerol solutions. The silica particles represent cells and their processes, and the aqueous phase represents the ECS. This model allowed us to vary ECS size by changing the density of silica microbeads, and ECS viscosity by changing aqueous-phase water/glycerol content. The inclusion of glycerol permitted approximate matching of silica and aqueous-phase refractive indices to minimize light scattering from the silica microbeads. Under these conditions, the silica microbeads appeared dark, with brightly fluorescent surrounding aqueous-phase "ECS" (Fig. 6*B*).

This simple in vitro model reproduced semiquantitatively the changes in macromolecular diffusion in the ECS observed in vivo during cytotoxic and vasogenic brain swelling. Representative fluorescence recovery curves are shown in Figure 6*B*. An increase in the size of the space between particles produced by reduction in silica density (as seen in vasogenic edema) caused a reduction in $t_{1/2}$. Increased silica density with corresponding reduction of aqueous-phase volume (as seen in cytotoxic edema) not only slowed diffusion, but also prevented complete recovery of fluorescence (Fig. 6*C*). A threshold phenomenon was seen as found in brain in vivo, in which diffusion becomes greatly slowed and restricted when aqueous-phase volume is reduced over a relatively small range. To investigate the interdependence of ECS geometric and diffusive properties, we carried out photobleaching measurements at constant silica density but different

aqueous-phase viscosities. Figure 6*D* shows increased $t_{1/2}$ with increasing aqueous-phase viscosity, as expected. However, the ratio of $t_{1/2}$ in the presence of the silica microbeads to $t_{1/2}$ in the absence of the microbeads was constant, indicating that overall diffusion is slowed independently by geometric constraints and aqueous-phase viscosity.

DISCUSSION

Using a novel, minimally invasive technique, we found that vasogenic brain edema enhanced the diffusion of FITC-dextran in the ECS, whereas cytotoxic edema slowed its diffusion and prevented complete recovery of signal. These findings suggest that the presence of excess fluid in brain ECS in vasogenic edema expands the ECS, whereas cell swelling in cytotoxic edema contracts the ECS. In both models of vasogenic brain edema used here, expansion of ECS occurred in brain distant from the lesion. Increased brain water content remote from the lesion site is a common finding in models of vasogenic brain edema, such as brain tumor in monkey and cat (20, 21), and cold injury in rabbit and cat (20, 22). It probably arises due to the flow of edema fluid away from the site of its formation along white matter tracts. The current setup does not allow monitoring from white matter, which is expected to show larger change in ECS diffusion during vasogenic edema than gray matter.

Our results concur with diffusion tensor magnetic resonance data from cat brain (23), which showed that in vasogenic edema (induced by cortical freeze lesion) the apparent diffusion coefficient (ADC) increased, but in cytotoxic edema (induced by middle cerebral occlusion) ADC decreased. In many clinical situations, such as traumatic brain injury (24) and meningitis (25), vasogenic and cytotoxic edema are thought to coexist with different spatial and temporal profiles. Measurement of macromolecule diffusion in the ECS by cortical photobleaching should be useful in delineating, spatially and temporally, the relative roles of these opposing mechanisms in vivo.

Implantation of melanoma cells and rapid growth of a solid melanoma tumor mass produced marked changes in FITC-dextran diffusion in brain within, nearby, and at a distance away from the tumor. The increased ECS diffusion in normal brain distant from the tumor probably reflects ECS expansion caused by vasogenic edema. This observation is supported by a magnetic resonance diffusion tensor imaging study that showed significantly elevated mean diffusivity adjacent to human high grade gliomas and brain metastases in vivo (26). These peritumoral regions of interest were noted to have high signal on T2 sequence, in a pattern suggestive of vasogenic brain edema.

We also found remarkably slowed FITC-dextran diffusion in the ECS within the tumor mass, in agreement with TMA^+ experiments reporting increased tortuosity in resected malignant human brain tumors (27), and diffusion-weighted magnetic resonance imaging showing low ADC inside aggressive human brain tumors in vivo (28, 29). Impaired macromolecular diffusion in the ECS in aggressive tumors has been proposed to result from a combination of hypercellularity, reduced ECS volume, and overproduction of extracellular matrix components (30, 31). In the peritumoral astrogliotic rim, we found slowed FITC-dextran diffusion, probably as a consequence of high cellularity, with a dense entanglement of reactive astroglial processes and increased extracellular matrix. Slowed TMA^+ diffusion and reduced ADC have been reported in a stab-injury model of rat cortical astrogliosis associated with up-regulation of chondroitin sulfate proteoglycan (32).

We suggest that reactive astrogliosis around brain lesions is a protective response by inhibiting ECS diffusion and thus limiting the flow of vasogenic edema fluid from the tumor bed into the brain parenchyma. This hypothesis is in line with other studies that showed that ablation of reactive astrocytes increased the extent of tissue damage after brain or spinal cord injury (33, 34).

Dexamethasone, a widely used treatment for brain tumor edema, is thought to reduce tumor capillary leak (35–37). In cultured endothelial cells, dexamethasone caused up-regulation and dephosphorylation of tight junction proteins, including occludin and ZO-1 (18, 19, 38). In a rat brain tumor model, dexamethasone reduced the response of the vasculature to tumor-derived permeability factors, including vascular endothelial growth factor (VEGF), and reduced VEGF expression by tumor cells. We found here that the increased FITC-dextran diffusion in the ECS away from a brain tumor was reduced to that in normal brain after dexamethasone treatment. Dexamethasone did not affect FITC-dextran diffusion in contralateral brain, showing that dexamethasone itself did not affect ECS properties. The simplest interpretation of these results is the reduction of tumor-associated capillary fluid leak after dexamethasone; however, possible alterations in extracellular matrix composition may also play a role in the dexamethasone effect. These findings agree with diffusion tensor magnetic resonance data obtained from humans with primary intracranial tumors before and 48–72 h after dexamethasone treatment (39), where dexamethasone reduced mean diffusivity inside the tumor and adjacent edematous brain in 50% of the patients.

Cortical photobleaching revealed reduced FITC-dextran diffusion in the ECS in cytotoxic brain edema produced by chemical hypoxia and apnea, in accord with results from other models of cytotoxic edema including water intoxication, glutamate excitotoxicity and chemoconvulsant-induced seizures (14). The increased $t_{1/2}$ was associated with incomplete recovery of fluorescence, probably due to microcompartmentalization of the ECS (40). Cortical photobleaching is likely to be more sensitive in detecting cell swelling than ICP, which only rises when the functional compliance of intracranial compartments has been exceeded. Also, in some conditions such as early hypoxia or seizures, there is a redistribution of water from the ECS into the intracellular compartment without a net increase in brain water content. In such cases, ICP and total brain water content may remain normal, but macromolecule diffusion in the ECS would be slowed.

Diffusion of macromolecules in brain ECS (D_{ecs}) is slower than in solution (D_o). The degree of slowing has been expressed as "tortuosity" defined as $(D_o/D_{ecs})^{1/2}$ (41). To better understand the molecular determinants of tortuosity, we modeled the complex geometry of brain ECS with silica particles suspended in a fluorescent water-glycerol matrix. Tortuosity depended on the size and and viscosity of the ECS. Below a threshold aqueous-phase volume fraction, the ECS abruptly lost its continuity and became microcompartmentalized, associated with failure of the extracellular fluorescence to recover after photobleaching. In the brain, microcompartmentalization is a catastrophic event in which macromolecule diffusion in the ECS becomes highly restricted. Consequently, clearance of metabolites and toxic components such as potassium and glutamate from the ECS is greatly reduced, potentially leading to cell death. Interestingly, although data in vivo and in the silica model were qualitatively similar, microcompartmentalization occurred at a higher ECS volume in the silica model than in brain. We suggest that the brain has evolved mechanisms to resist microcompartmentalization. For

example, ECS matrix components may maintain cell-cell spacing during cell swelling, a feature that is not reproduced in the silica microbead model where direct bead-bead contact was not prevented.

Another conclusion from the silica microbead experiments was the independence of the two principal determinants of ECS diffusion, geometric restriction and intrinsic matrix diffusivity. It is easily appreciated that doubling ECS viscosity without changing geometry would reduce twofold the observed rate of diffusion. The independence of geometry and intrinsic diffusivity was validated experimentally and analyzed theoretically in photobleaching measurements of small molecule diffusion in cytoplasm (42) and other intracellular compartments (43). A similar conclusion about the independence of geometry and intrinsic diffusivity was reached for brain ECS on theoretical grounds, by applying principles of integral geometry to random assemblies of space-filling obstacles (44). This model, however, does not take into account ECS microcompartmentalization, which becomes prominent as ECS volume decreases. It has been suggested that microcompartmentalization may also occur when cells shrink, if the resulting change in cell shape is nonuniform (45).

Macromolecular diffusion in brain ECS is important in drug delivery to swollen brain associated with brain tumor, head injury, and stroke. Systemically introduced drugs must cross the blood-brain barrier and travel through the ECS before reaching their target cells (46). The ECS diffusive barrier may be particularly rate-limiting in gene and immune therapies, which rely on delivery of high molecular weight agents. Hyaluronidase (47) and collagenase (31) may increase chemosensitivity of tumors by increasing intrinsic extracellular matrix diffusivity. Although dexamethasone alleviates symptoms by reducing brain tumor edema, it might also compromise the delivery of chemotherapeutic agents into the tumor by reducing brain ECS volume and macromolecular diffusivity. Therapeutic macromolecules introduced into the ECS may paradoxically worsen outcome by becoming trapped, in effect promoting ECS microcompartmentalization (40). In general, drug delivery by ECS diffusion is expected to be slow in regions primarily affected by cytotoxic edema, but fast in regions where vasogenic edema predominates. Investigations of the diffusion of DNA, protein and liposome macromolecules in models of brain swelling will be needed to validate these ideas. This should now be feasible using cortical fluorescence recovery after photobleaching.

ACKNOWLEDGMENTS

We thank Liman Qian for mouse breeding and care. This work was funded by grants DK35124, EY13574, HL59198, EB00415, and HL73856 from the National Institutes of Health, and a Research Development Program grant from the Cystic Fibrosis Foundation (to ASV) and by a Wellcome Trust Clinician Scientist Fellowship (to MCP sponsored by Sanjeev Krishna).

REFERENCES

1. Papadopoulos, M. C., Davies, D. C., Moss, R. F., Tighe, D., and Bennett, E. D. (2000) Pathophysiology of septic encephalopathy: a review. *Crit. Care Med.* **28,** 3019–3024

2. Kimelberg, H. K. (1995) Current concepts of brain edema: review of laboratory investigations. *J. Neurosurg.* **83,** 1051–1059

3. Fishman, R. A. (1975) Brain edema. *N. Engl. J. Med.* **293,** 706–711

4. Papadopoulos, M. C., Saadoun, S., Binder, D. K., Manley, G. T., Krishna, S., and Verkman, A. S. (2004) Molecular mechanisms of brain tumor edema. *Neuroscience*, **129,** 1011–1020

5. Manley, G. T., Binder, D. K., Papadopoulos, M. C., and Verkman, A. S. (2004) New insights into water transport and edema in the central nervous system from phenotype analysis of AQP4-null mice. *Neuroscience*, **129,** 983–991

6. Klatzo, I. (1994) Evolution of brain edema concepts. *Acta Neurochir. Suppl. (Wien)* **60,** 3–6

7. Weed, L. H., and McKibben, P. S. (1919) Experimental alteration of brain bulk. *Am. J. Physiol.* **48,** 531–538

8. Jelsma, R., and Bucy, P. C. (1967) The treatment of glioblastoma multiforme of the brain. *J. Neurosurg.* **27,** 388–400

9. Ghajar, J. (2000) Traumatic brain injury. *Lancet* **356,** 923–929

10. Manley, G. T., Fujimura, M., Ma, T., Noshita, N., Filiz, F., Bollen, A. W., Chan, P., and Verkman, A. S. (2000) Aquaporin-4 deletion in mice reduces brain edema after acute water intoxication and ischemic stroke. *Nat. Med.* **6,** 159–163

11. Papadopoulos, M. C., Manley, G. T., Krishna, S., and Verkman, A. S. (2004) Aquaporin-4 facilitates reabsorption of excess fluid in vasogenic brain edema. *FASEB J.* **18,** 1291–1293

12. Nicholson, C., Chen, K. C., Hrabetova, S., and Tao, L. (2000) Diffusion of molecules in brain extracellular space: theory and experiment. *Prog. Brain Res.* **125,** 129–154

13. Nicholson, C. (1992) Quantitative analysis of extracellular space using the method of TMA+ iontophoresis and the issue of TMA+ uptake. *Can. J. Physiol. Pharmacol.* **70, Suppl,** S314–S322

14. Binder, D. K., Papadopoulos, M. C., Haggie, P. M., and Verkman, A. S. (2004) In vivo measurement of brain extracellular space diffusion by cortical surface photobleaching. *J. Neurosci.* **24,** 8049–8056

15. Jayaraman, S., Joo, N. S., Reitz, B., Wine, J. J., and Verkman, A. S. (2001) Submucosal gland secretions in airways from cystic fibrosis patients have normal [Na(+)] and pH but elevated viscosity. *Proc. Natl. Acad. Sci. USA* **98,** 8119–8123

16. Feder, T. J., Brust-Mascher, I., Slattery, J. P., Baird, B., and Webb, W. W. (1996) Constrained diffusion or immobile fraction on cell surfaces: a new interpretation. *Biophys. J.* **70,** 2767–2773

17. Ito, U., Tomita, H., Tone, O., Masaoka, H., and Tominaga, B. (1994) Peritumoral edema in meningioma: a contrast enhanced CT study. *Acta Neurochir. Suppl. (Wien)* **60,** 361–364

18. Antonetti, D. A., Wolpert, E. B., DeMaio, L., Harhaj, N. S., and Scaduto, R. C., Jr. (2002) Hydrocortisone decreases retinal endothelial cell water and solute flux coincident with increased content and decreased phosphorylation of occludin. *J. Neurochem.* **80,** 667–677

19. Underwood, J. L., Murphy, C. G., Chen, J., Franse-Carman, L., Wood, I., Epstein, D. L., and Alvarado, J. A. (1999) Glucocorticoids regulate transendothelial fluid flow resistance and formation of intercellular junctions. *Am. J. Physiol.* **277,** C330–C342

20. Bothe, H. W., Bodsch, W., and Hossmann, K. A. (1984) Relationship between specific gravity, water content, and serum protein extravasation in various types of vasogenic brain edema. *Acta Neuropathol. (Berl.)* **64,** 37–42

21. Yamada, K., Bremer, A. M., and West, C. R. (1979) Effects of dexamethasone on tumor-induced brain edema and its distribution in the brain of monkeys. *J. Neurosurg.* **50,** 361–367

22. Pash, M. P., and Tweed, W. A. (1979) Tissue albumin and water content in the early stages of vasogenic brain edema formation. *Can. J. Neurol. Sci.* **6,** 423–426

23. Kuroiwa, T., Nagaoka, T., Miyasaka, N., Akimoto, H., Zhao, F., Yamada, I., Ueki, M., and Ichinose, S. (2000) Time course of trace of diffusion tensor [Trace(D)] and histology in brain edema. *Acta Neurochir. Suppl. (Wien)* **76,** 191–194

24. Ito, J., Marmarou, A., Barzo, P., Fatouros, P., and Corwin, F. (1996) Characterization of edema by diffusion-weighted imaging in experimental traumatic brain injury. *J. Neurosurg.* **84,** 97–103

25. Nau, R., and Bruck, W. (2002) Neuronal injury in bacterial meningitis: mechanisms and implications for therapy. *Trends Neurosci.* **25,** 38–45

26. Lu, S., Ahn, D., Johnson, G., and Cha, S. (2003) Peritumoral diffusion tensor imaging of high-grade gliomas and metastatic brain tumors. *AJNR Am. J. Neuroradiol.* **24,** 937–941

27. Vargova, L., Homola, A., Zamecnik, J., Tichy, M., Benes, V., and Sykova, E. (2003) Diffusion parameters of the extracellular space in human gliomas. *Glia* **42,** 77–88

28. Kono, K., Inoue, Y., Nakayama, K., Shakudo, M., Morino, M., Ohata, K., Wakasa, K., and Yamada, R. (2001) The role of diffusion-weighted imaging in patients with brain tumors. *AJNR Am. J. Neuroradiol.* **22,** 1081–1088

29. Sugahara, T., Korogi, Y., Ge, Y., Shigematsu, Y., Liang, L., Yoshizumi, K., Kitajima, M., and Takahashi, M. (1999) Contrast enhancement of intracranial lesions: conventional T1-weighted spin-echo versus fast spin-echo MR imaging techniques. *AJNR Am. J. Neuroradiol.* **20,** 1554–1559

30. Pluen, A., Boucher, Y., Ramanujan, S., McKee, T. D., Gohongi, T., di Tomaso, E., Brown, E. B., Izumi, Y., Campbell, R. B., Berk, D. A., et al. (2001) Role of tumor-host interactions in interstitial diffusion of macromolecules: cranial vs. subcutaneous tumors. *Proc. Natl. Acad. Sci. USA* **98,** 4628–4633

31. Netti, P. A., Berk, D. A., Swartz, M. A., Grodzinsky, A. J., and Jain, R. K. (2000) Role of extracellular matrix assembly in interstitial transport in solid tumors. *Cancer Res.* **60,** 2497–2503

32. Vorisek, I., Hajek, M., Tintera, J., Nicolay, K., and Sykova, E. (2002) Water ADC, extracellular space volume, and tortuosity in the rat cortex after traumatic injury. *Magn. Reson. Med.* **48,** 994–1003

33. Faulkner, J. R., Herrmann, J. E., Woo, M. J., Tansey, K. E., Doan, N. B., and Sofroniew, M. V. (2004) Reactive astrocytes protect tissue and preserve function after spinal cord injury. *J. Neurosci.* **24,** 2143–2155

34. Bush, T. G., Puvanachandra, N., Horner, C. H., Polito, A., Ostenfeld, T., Svendsen, C. N., Mucke, L., Johnson, M. H., and Sofroniew, M. V. (1999) Leukocyte infiltration, neuronal degeneration, and neurite outgrowth after ablation of scar-forming, reactive astrocytes in adult transgenic mice. *Neuron* **23,** 297–308

35. Koehler, P. J. (1995) Use of corticosteroids in neuro-oncology. *Anticancer Drugs* **6,** 19–33

36. Ito, U., Reulen, H. J., Tomita, H., Ikeda, J., Saito, J., and Maehara, T. (1990) A computed tomography study on formation, propagation, and resolution of edema fluid in metastatic brain tumors. *Adv. Neurol.* **52,** 459–468

37. Ito, U., Reulen, H. J., Tomita, H., Ikeda, J., Saito, J., and Maehara, T. (1988) Formation and propagation of brain oedema fluid around human brain metastases. A CT Study. *Acta Neurochir. (Wien)* **90,** 35–41

38. Romero, I. A., Radewicz, K., Jubin, E., Michel, C. C., Greenwood, J., Couraud, P. O., and Adamson, P. (2003) Changes in cytoskeletal and tight junctional proteins correlate with decreased permeability induced by dexamethasone in cultured rat brain endothelial cells. *Neurosci. Lett.* **344,** 112–116

39. Bastin, M. E., Delgado, M., Whittle, I. R., Cannon, J., and Wardlaw, J. M. (1999) The use of diffusion tensor imaging in quantifying the effect of dexamethasone on brain tumours. *Neuroreport* **10,** 1385–1391

40. Hrabetova, S., Hrabe, J., and Nicholson, C. (2003) Dead-space microdomains hinder extracellular diffusion in rat neocortex during ischemia. *J. Neurosci.* **23,** 8351–8359

41. Nicholson, C., and Sykova, E. (1998) Extracellular space structure revealed by diffusion analysis. *Trends Neurosci.* **21,** 207–215

42. Kao, H. P., Abney, J. R., and Verkman, A. S. (1993) Determinants of the translational mobility of a small solute in cell cytoplasm. *J. Cell Biol.* **120,** 175–184

43. Verkman, A. S. (2002) Solute and macromolecule diffusion in cellular aqueous compartments. *Trends Biochem. Sci.* **27,** 27–33

44. Rusakov, D. A., and Kullmann, D. M. (1998) Geometric and viscous components of the tortuosity of the extracellular space in the brain. *Proc. Natl. Acad. Sci. USA* **95,** 8975–8980

45. Chen, K. C., and Nicholson, C. (2000) Changes in brain cell shape create residual extracellular space volume and explain tortuosity behavior during osmotic challenge. *Proc. Natl. Acad. Sci. USA* **97,** 8306–8311

46. Jain, R. K. (1998) The next frontier of molecular medicine: delivery of therapeutics. *Nat. Med.* **4,** 655–657

47. Croix, B. S., Rak, J. W., Kapitain, S., Sheehan, C., Graham, C. H., and Kerbel, R. S. (1996) Reversal by hyaluronidase of adhesion-dependent multicellular drug resistance in mammary carcinoma cells. *J. Natl. Cancer Inst.* **88,** 1285–1296

Received August 5, 2004; accepted November 3, 2004.

Fig. 1

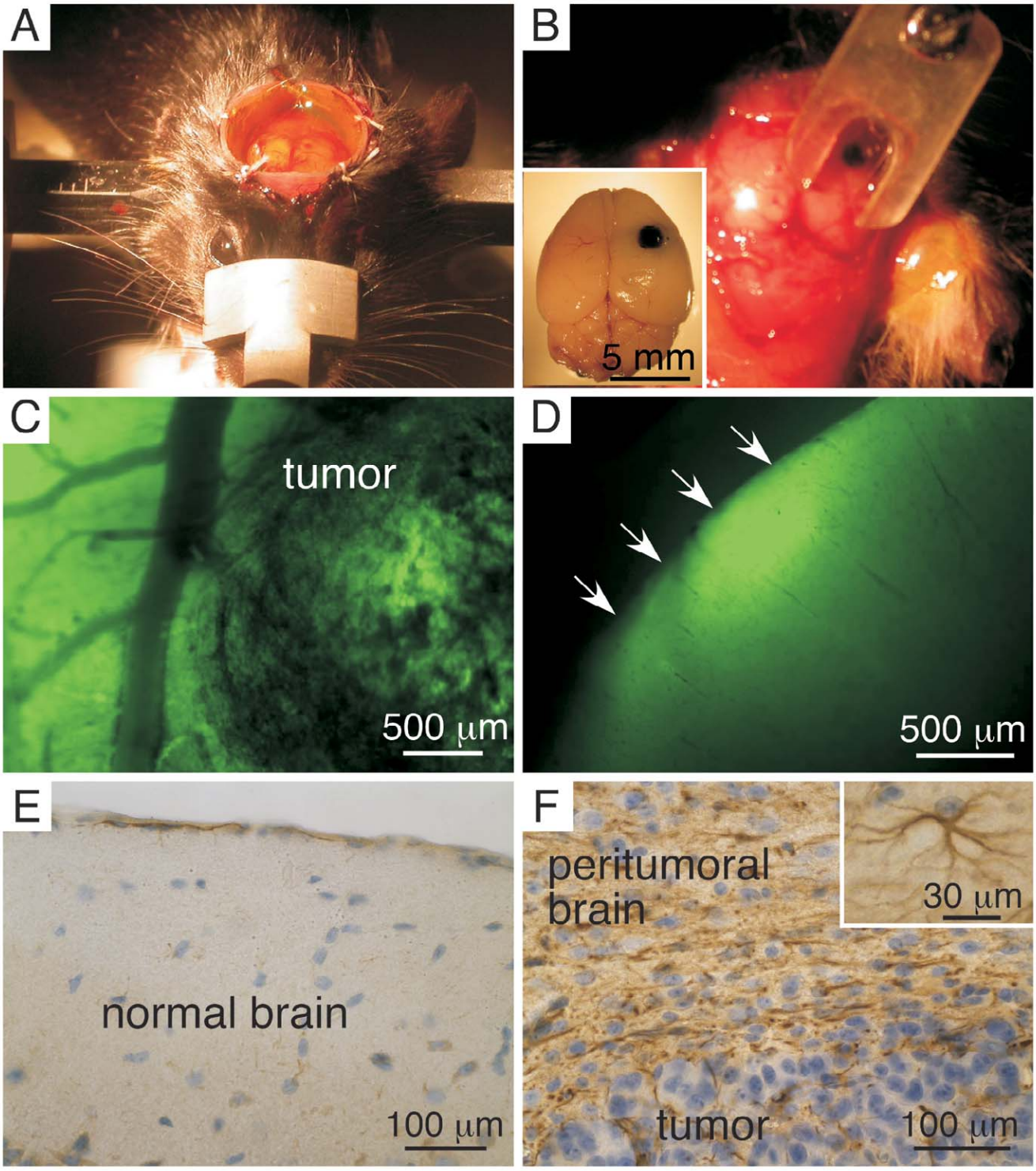

Figure 1. Experimental setup. ***A)*** Mouse head immobilized in stereotactic frame. After bilateral craniectomy, the scalp was sutured to a plastic ring as a reservoir for the dye-containing aCSF. ***B)*** During recording of fluorescence, a coverslip appended to a side arm gently rested on the exposed dura to dampen cardiorespiratory oscillations. The melanoma is visible on the brain surface through the coverslip (also seen in inset). ***C)*** Fluorescent brain surface after dye loading. ***D)*** Cut section (150 μm thick) of brain immediately after dye loading showing fluorescently stained parenchyma with strongest signal in superficial cortical layers. ***E, F)*** Brain was immunostained for GFAP with hematoxylin counterstain. Note greater cell density in tumor and peritumoral brain in ***F*** compared with normal brain in ***E***. The peritumoral brain also contains many cell processes from reactive astrocytes (***F***, inset).

Fig. 2

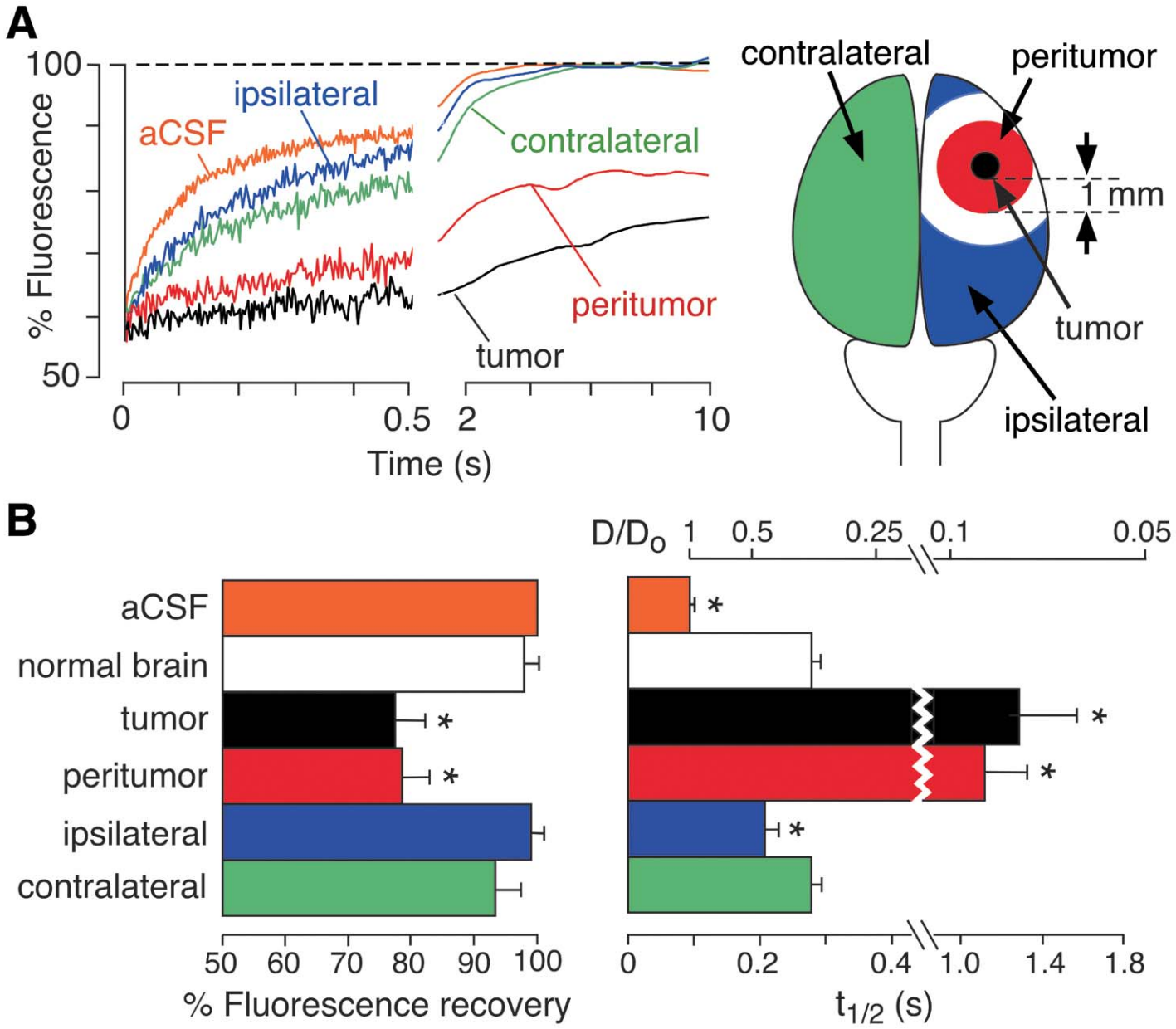

Figure 2. ECS expansion in tumor vasogenic edema. ***A) Left***: Representative fluorescence recovery curves at different locations with respect to the tumor. ***Right***: Signal was recorded from the tumor (black), peritumoral brain (red, <1 mm away from tumor), ipsilateral brain (blue, >2 mm away from tumor), and contralateral brain (green). ***B)*** Analysis of photobleaching data. ***Left***: Percentage fluorescence recovery at 10 s after photobleaching. ***Right***: Recovery half-times ($t_{1/2}$) and corresponding relative diffusion coefficients (D/D_o). Mean ± SE (n=7–10, *P<0.05 compared with normal brain).

Fig. 3

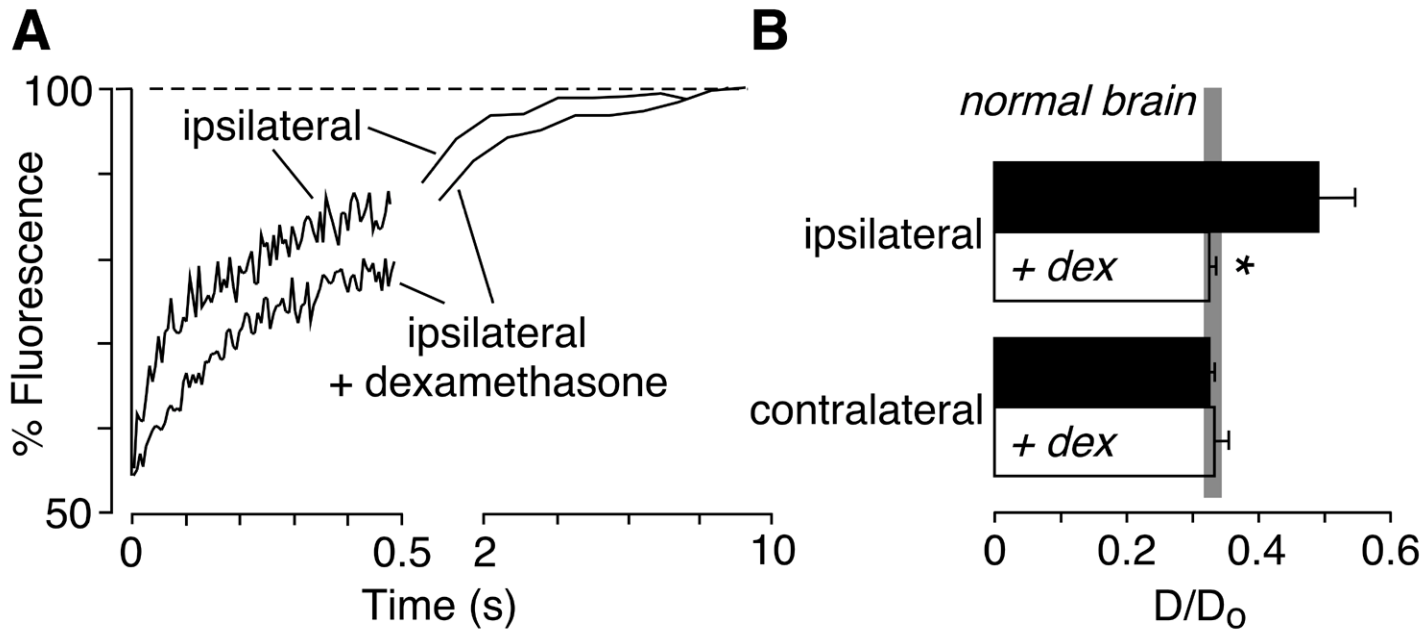

Figure 3. Reduced ECS expansion in brain tumor vasogenic edema after dexamethasone administration. ***A)*** Representative fluorescence recovery curves ipsilateral and contralateral brain parenchyma in control and dexamethasone (dex)-treated mice. ***B)*** Averaged data summarized as in **Figure 2*B*** (n=6–7, *P<0.05).

Fig. 4

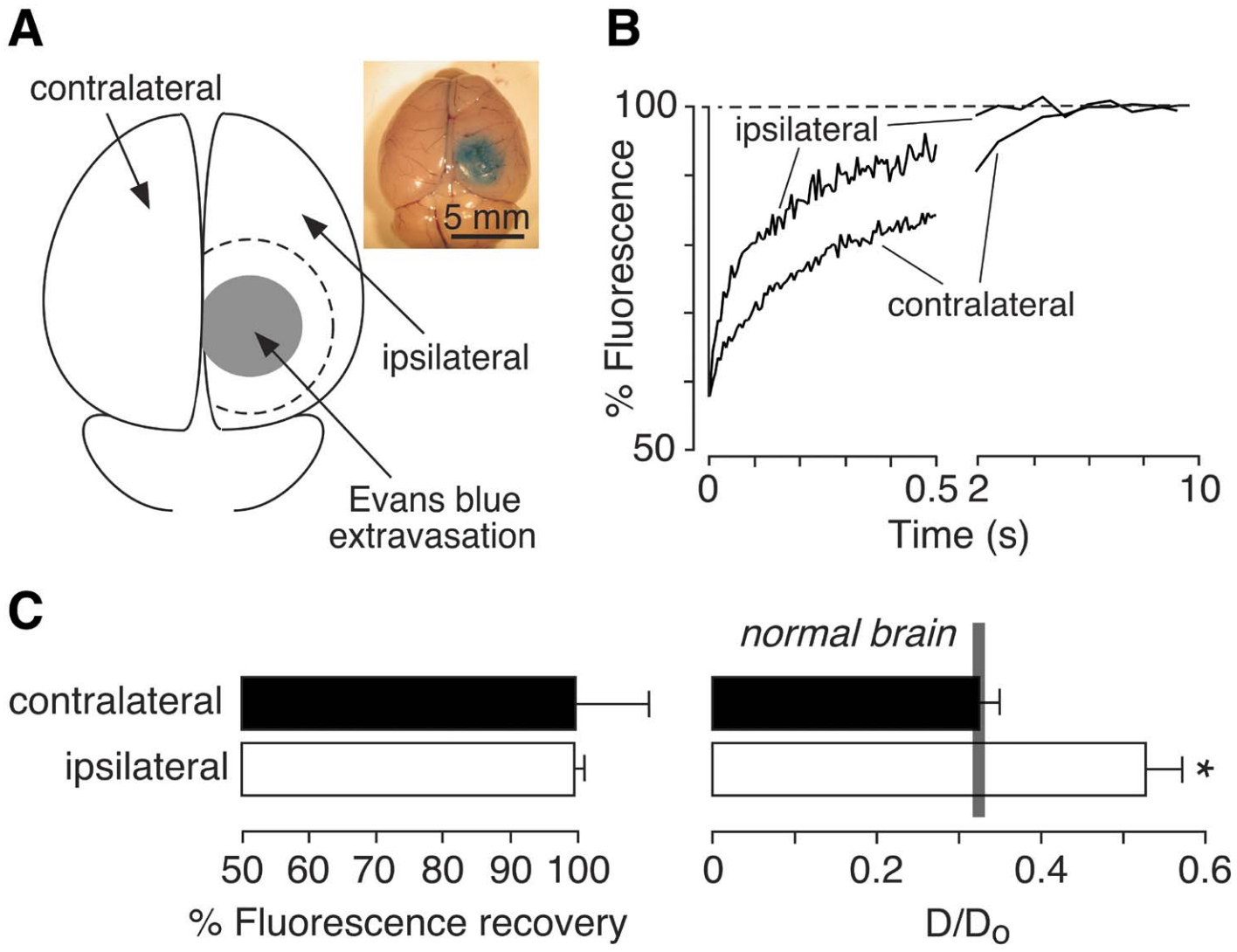

Figure 4. ECS expansion in vasogenic edema produced by cortical-freeze injury. ***A)*** Cortical areas in relation to the cold lesion. Ipsilateral brain taken as >1 mm away from the injured site. Inset: Extravasation of Evans blue dye at the site of cortical-freeze injury. ***B)*** Representative fluorescence recovery curves in ipsilateral and contralateral hemispheres. ***C)*** Summary of percentage fluorescence recovery (***left***) and D/D_o (***right***) for contralateral (n=3) and ipsilateral (n=6) brain (*P<0.05).

Fig. 5

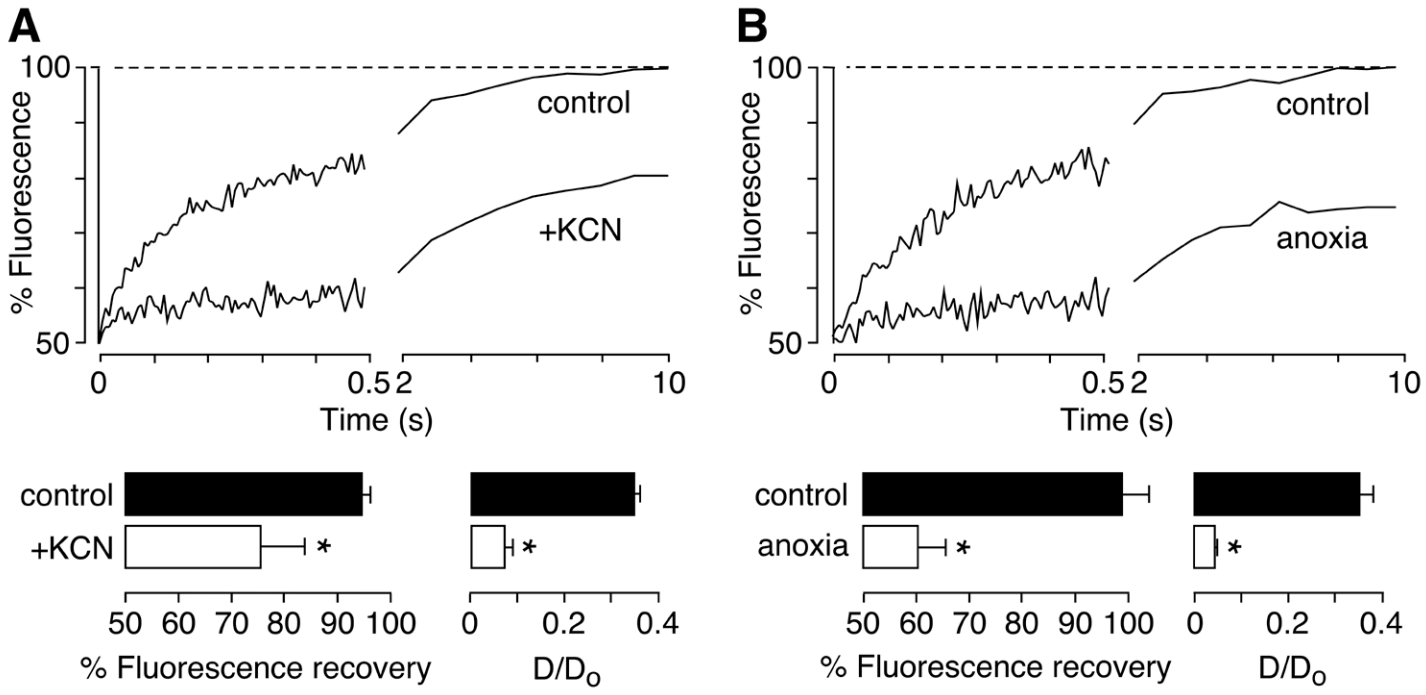

Figure 5. Cytotoxic edema slows diffusion in brain ECS. ***A) Top***: Fluorescence recovery curves before and 15 min after cerebral cortical hypoxia produced by topical potassium cyanide (KCN). ***Bottom***: Summary of percentage recovery and D/D_o (n=5). ***B) Top***: Fluorescence recovery curves before and 5 min after global anoxia produced by anesthetic overdose causing apnea. ***Bottom***: Summary of percentage recovery and D/D_o (n=8, *P<0.05).

Fig. 6

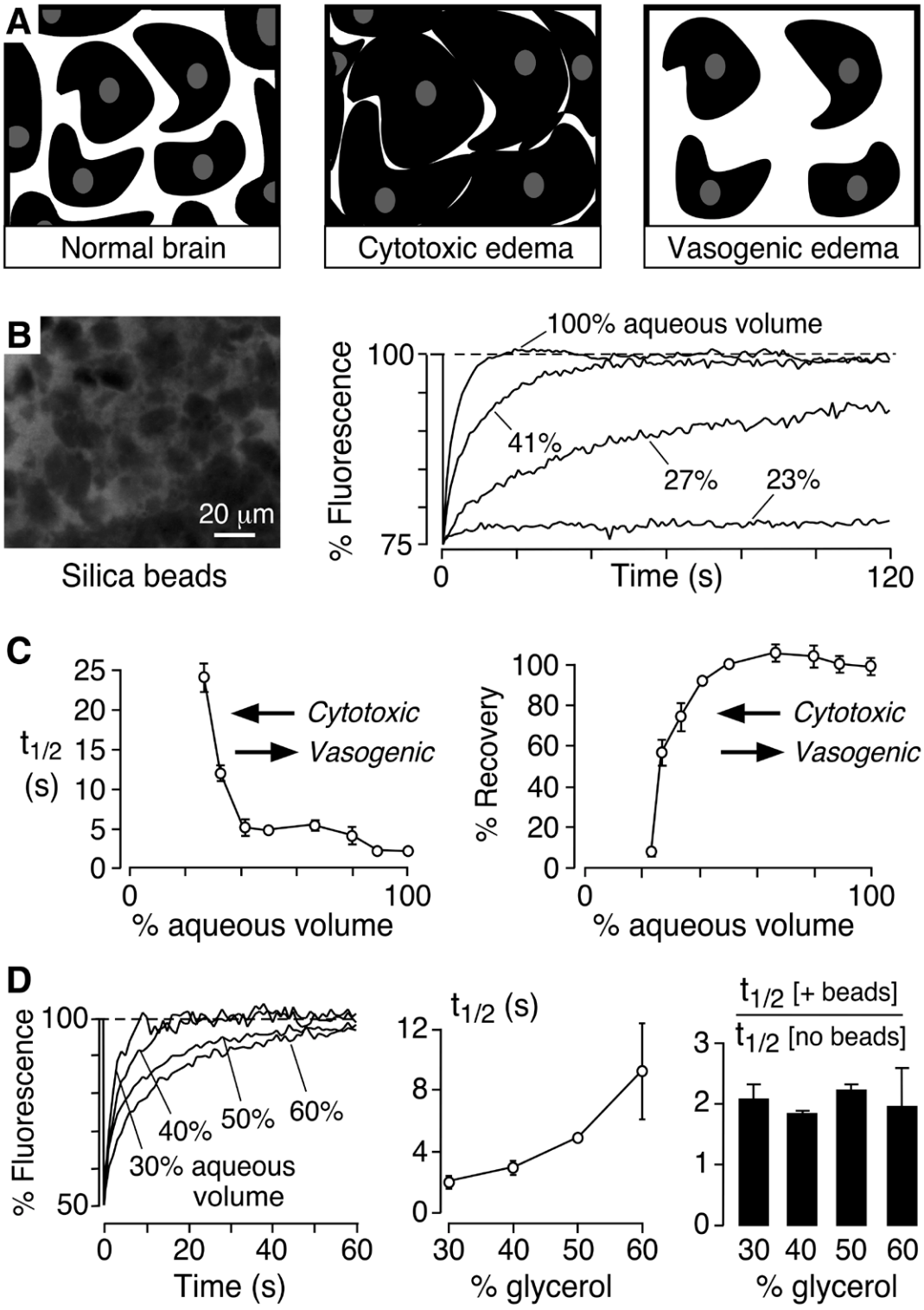

Figure 6. Diffusion in an in vitro model of brain ECS. ***A)*** Schematic of cells (black) and extracellular space (white) in normal brain (***left***), cytotoxic edema (***middle***), and vasogenic edema (***right***). See text for explanation. ***B) Left***: Fluorescence micrograph of fused silica microspheres (dark regions) suspended in aCSF (containing glycerol and fluorescein-dextran). ***Right***: Fluorescence recovery curves in suspensions of microbeads in aCSF containing 50% glycerol. ***C)*** Summary of $t_{1/2}$ (***left***) and percentage recovery (***right***) (n=3 per point). Decreasing/increasing aqueous solution volume mimics cytotoxic/vasogenic brain edema, respectively. ***D) Left***: Fluorescence recovery curves of FITC-dextran in aCSF containing a 50% suspension of microbeads at indicated glycerol concentrations. ***Middle***: Summary of $t_{1/2}$ (mean ± SE, n=3 per point). ***Right***: Ratio of $t_{1/2}$ in the presence of beads vs. $t_{1/2}$ in same solution without beads.